JACS Au
AN OPEN ACCESS JOURNAL OF THE AMERICAN CHEMICAL SOCIETY

pubs.acs.org/jacsau
Article

Sequential Pore Functionalization in MOFs for Enhanced Carbon Dioxide Capture

Ankit K. Yadav, Andrzej Gładysiak, Ah-Young Song, Lei Gan, Casey R. Simons, Nawal M. Alghoraibi, Ammar H. Alahmed, Mourad Younes, Jeffrey A. Reimer, Hongliang Huang,* José G. Planas, and Kyriakos C. Stylianou*

Cite This: *JACS Au* 2024, 4, 4833−4843
Read Online

ABSTRACT: The capture of carbon dioxide (CO_2) is crucial for reducing greenhouse emissions and achieving net-zero emission goals. Metal−organic frameworks (MOFs) present a promising solution for carbon capture due to their structural adaptability, tunability, porosity, and pore modification. In this research, we explored the use of a copper (Cu(II))-based MOF called ***m*CBMOF-1**. After activation, ***m*CBMOF-1** generates one-dimensional channels with square cross sections, featuring sets of four Cu(II) open metal sites spaced by 6.042 Å, allowing strong interactions with coordinating molecules. To investigate this capability, ***m*CBMOF-1** was exposed to ammonia (NH_3) gas, resulting in hysteretic NH_3 isotherms indicative of strong interactions between Cu(II) and NH_3. At 150 mbar and 298 K, the NH_3-loaded (∼1 mmol/g) material exhibited a 106% increase in CO_2 uptake compared to that of the pristine ***m*CBMOF-1**. Carbon-13 solid-state nuclear magnetic resonance spectra and density functional theory calculations confirmed that the sequential loading of NH_3 followed by CO_2 adsorption generated a copper−carbamic acid complex within the pores of ***m*CBMOF-1**. Our study highlights the effectiveness of sequential pore functionalization in MOFs as an attractive strategy for enhancing the interactions of MOFs with small molecules such as CO_2.

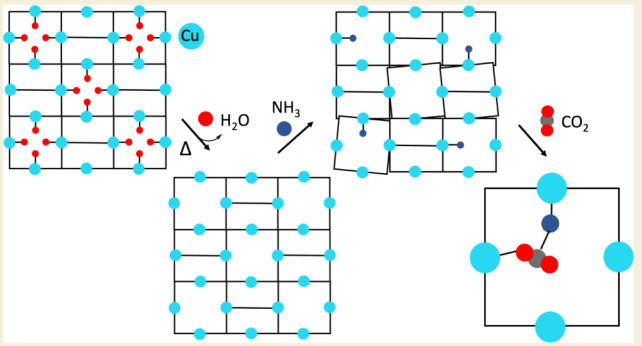

KEYWORDS: *metal−organic frameworks, ammonia, postsynthetic modification, carbon dioxide, capture*

INTRODUCTION

Carbon dioxide (CO_2) emissions into the atmosphere contribute to the greenhouse effect[1,2] caused by the absorption of infrared rays reflected by the Earth's surface.[3,4] Uncontrolled greenhouse gas emissions into the atmosphere have played a pivotal role in global climate change.[5,6] According to the data from the Mauna Loa Observatory,[6] the atmospheric concentration of CO_2 reached 422.1 ppm in July 2023, marking a 31.9% increase from the 1950 level of 320 ppm and a 50.8% increase from preindustrial levels of 280 ppm.[7,8] Despite efforts to set a target of 350 ppm for global atmospheric CO_2 levels, CO_2 concentrations continue to rise.[9,10] In 2018, the Intergovernmental Panel on Climate Change[11] reported that surpassing a global temperature increase of 1.5 °C above the 20th-century average could lead to severe consequences, and crossing the 2.0 °C threshold might result in irreversible outcomes. Moreover, higher global temperatures are expected to exacerbate issues such food and water scarcity, potentially leading to increased poverty rates.[12,13] Carbon dioxide capture presents a promising solution to reduce the amount of CO_2 entering the atmosphere or remove CO_2 already emitted, such as through the use of Direct Air Capture systems, which were considered a viable option in many outlook scenarios and are essential in the IEA net-zero pathway. However, CO_2 capture technologies face challenges due to high costs associated with material limitations such as working capacity, degradation, or extensive energy demand. Therefore, the development of innovative approaches and new materials is crucial to capture of CO_2 effectively and economically.

Metal−organic frameworks (MOFs) are a class of porous materials composed of metal ions or clusters and organic linkers, which form extended structures. Their properties, which include exceptionally high surface areas,[14] tailored functionality,[15,16] and permanent porosity,[17,18] make them highly suitable for gas adsorption applications such as CO_2

Received: September 1, 2024
Revised: October 31, 2024
Accepted: November 4, 2024
Published: December 3, 2024

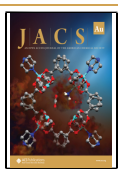

https://doi.org/10.1021/jacsau.4c00808
JACS Au 2024, 4, 4833−4843

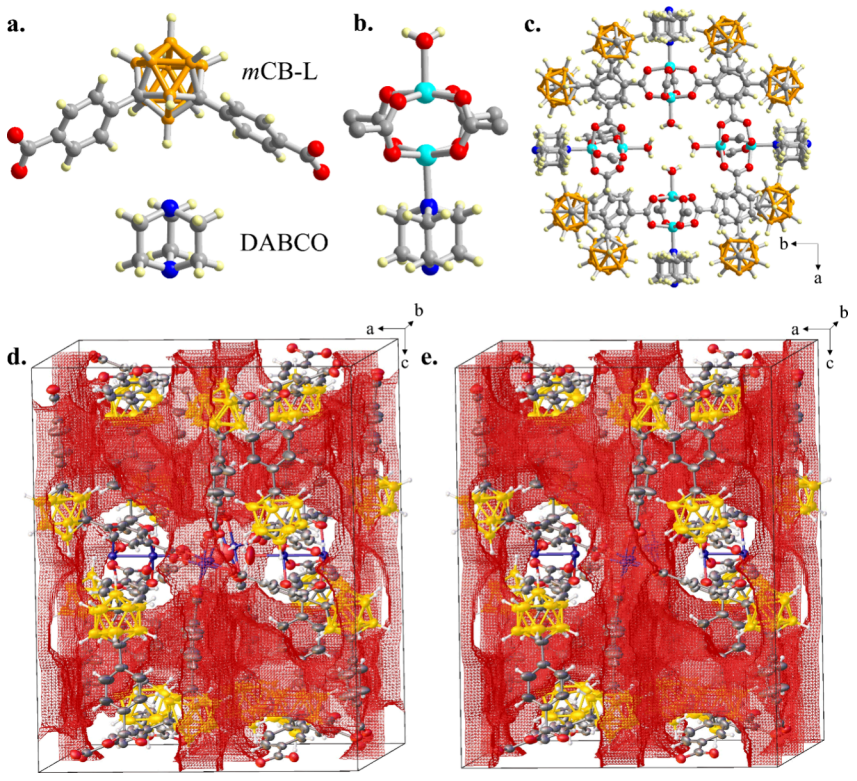

Figure 1. Structure representation of *m*CBMOF-1. (a) ***m*CBMOF-1** comprises a *meta*-carborane-dicarboxylate ligand and DABCO. (b) In ***m*CBMOF-1**, each Cu(II) is five coordinated, forming Cu_2-paddlewheels. The axial position for each Cu in the paddlewheel is distinct: Cu1 is bound to an aqua ligand, and Cu2 is bound to the N atom of DABCO. (c) The extended structure of ***m*CBMOF-1** illustrates the generation of the 4Cu site where each Cu is connected to an aqua ligand. (d) Three-dimensional ball and stick packing of ***m*CBMOF-1**. Red surfaces represent the accessible void within the unit cell. (e) The pore topology of ***m*CBMOF-1** after removal of the four aqua ligands bound to the 4Cu site. This results in the formation of an additional void channel extending along [001]. Atom color code: gray for C, red for O, blue for N, golden for B, sky blue for Cu, and pale yellow for H.

capture.[19,20] Several approaches have been explored to enhance the interaction between the pores of MOF adsorbents and CO_2.[21] One such approach involves the utilization of microporous (pore size <20 Å) and ultramicroporous (pore size <7 Å) MOFs, whose pores possess favorable shapes and sizes to facilitate host−guest interactions[11,22−24] effective for capturing CO_2 even in the presence of water vapor.[25] In a recent study, MIL-120, an ultramicroporous MOF, was employed for CO_2 capture, resulting in enhanced CO_2 uptake under humid conditions.[26] Another well-explored method of CO_2 capture enhancement involves the introduction of open metal sites through rational design, desolvation, or activation. Many MOFs, including those from the M-MOF-74 family (M = Mg, Mn, Fe, Co, Zn, Ni),[27,28] zirconium-based UiO-66,[29] and HKUST-1,[30] have achieved significant CO_2 uptakes using this approach.

Through careful design, either before or after their synthesis, the affinity of MOFs toward CO_2 can be significantly improved.[31−36] One key approach involves pore functionalization, wherein terminal uncoordinated functional groups such as $-NH_2$, −OH, and −COOH are introduced into the organic linker before MOF synthesis.[33,37−39] This results in MOFs with pores decorated with polarizable functional groups, thereby leading to increased CO_2 uptakes. In a study conducted by Arstad et al., the impact of an amino-substituted 1,4-benzene dicarboxylate ligand on the CO_2 uptake of three different MOFs (USO-1-Al, USO-2-Ni, and USO-3-In) was investigated.[40] Interestingly, in all three of the MOFs, the amino-substituted MOF exhibited higher CO_2 uptakes than their unfunctionalized counterparts. USO-2-Ni-NH_2 demonstrated the highest CO_2 uptake of 14 wt % (3.18 mmol/g) at 1 bar and 298 K, which represented a discernible increase from 10 wt % (2.27 mmol/g) for the unfunctionalized USO-2-Ni at the same conditions.[40] Other examples of such functionalized MOFs include CAU-1,[41] bio-MOF-11,[42] and NH_2-MIL-53(Al).[43]

The pore surface in MOFs can be modified postsynthesis.[33,37,44] Examples of such postsynthetic MOF functionalization include attaching alkylamines to open metal sites, which changes the CO_2 capture mechanism and significantly increases CO_2 uptake. Darunte et al. found that after loading the MIL-101(Cr) MOF with tris(2-aminoethyl)amine, the CO_2 uptake increased from ∼0.5 mmol/g in pristine MOF to ∼1.4 mmol/g in amine functionalized MOF at 150 mbar and 298 K.[45] Lyu et al. studied the amino acid functionalized MOF-808 for CO_2 capture in humid flue gas conditions, and they found that after loading glycine in the MOF, the CO_2 uptake increased from ∼0.2 mmol/g in the MOF-808 to ∼0.5 mmol/g in MOF-808-Gly at 150 mbar and 298 K.[46] Finally, the functionalization of the pores of Mg_2(dobpdc) with *N,N′*-dimethylethylenediamine resulted in about a 10-fold increase in the CO_2 uptake.[47−49] In this class of MOFs, CO_2 is not directly attached to open metal sites, replacing alkylamine molecules, but is instead cooperatively inserted in between the metal and the amine.

https://doi.org/10.1021/jacsau.4c00808
JACS Au 2024, 4, 4833−4843

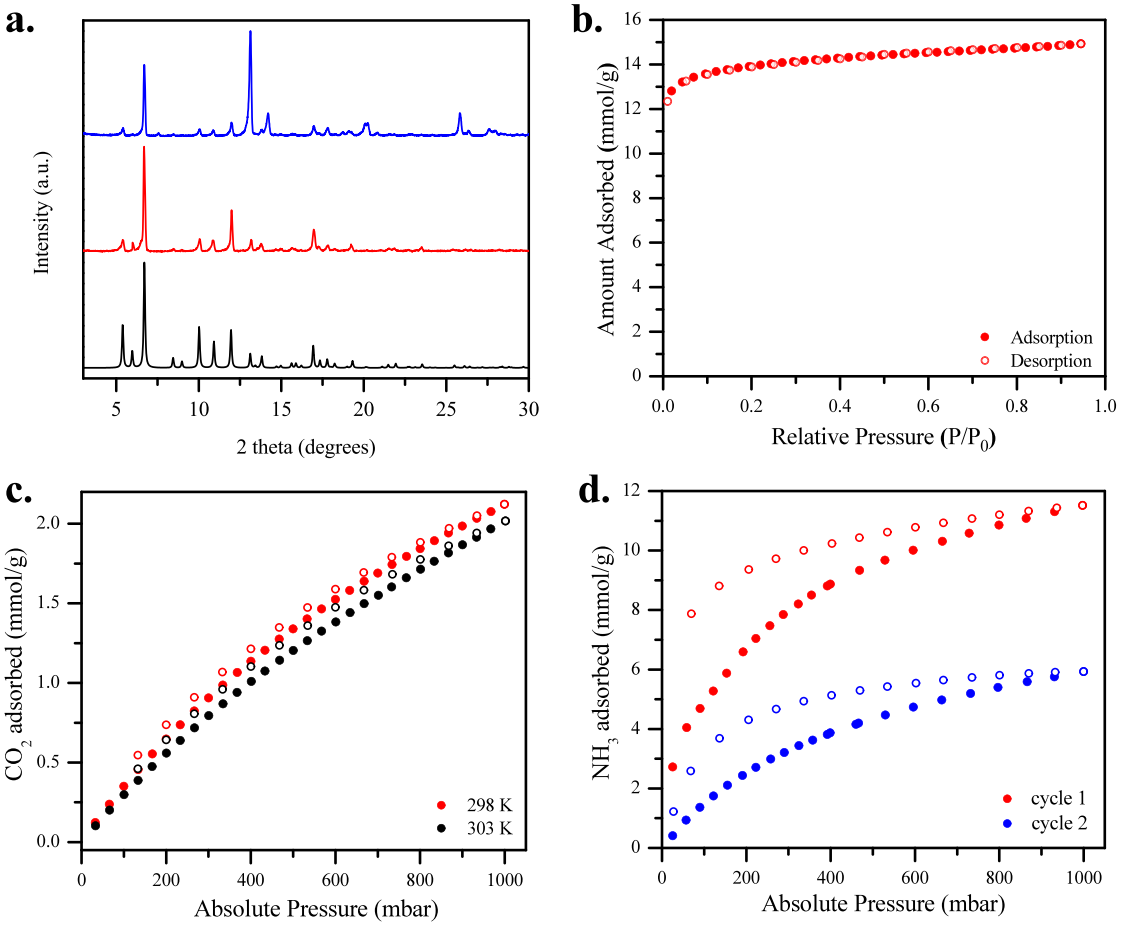

Figure 2. Solid-state characterization and sorption isotherms. (a) The powder X-ray diffraction patterns of as-made *m***CBMOF-1** (shown in red) are in excellent agreement with the pattern derived from the crystal structure of this material (simulated; shown in black), confirming the bulk phase purity of the MOF. The PXRD pattern of the ∼1 mmol NH_3-loaded *m***CBMOF-1** (shown in blue) indicates that the MOF retains its crystallinity. (b) The N_2 isotherm for the activated *m***CBMOF-1**, obtained at 77 K and 1 bar, indicates its microporous nature. (c) CO_2 isotherms for the activated *m***CBMOF-1** collected at 298 and 303 K. (d) Ammonia isotherms of *m***CBMOF-1**. The second NH_3 isotherm (colored in blue) was measured after *m***CBMOF-1** was reactivated following the first isotherm (colored in red). Filled symbols: adsorption; empty symbols: desorption.

In our study, we expand on the postsynthetic functionalization approach by coordinating gaseous ammonia (NH_3) to the open metal sites of a Cu(II)-based MOF, *m***CBMOF-1**, to enhance CO_2 adsorption. The activated MOF features four closely positioned, coordinatively unsaturated Cu(II) centers, which act as potent Lewis acidic sites known for their strong affinity for Lewis bases like NH_3. By anchoring NH_3 molecules within the MOF pores, we introduce a Lewis basic environment that enhances the selective capture of the Lewis acidic CO_2 molecules. This stepwise coordination of NH_3, followed by the coordination of CO_2, leads to the *in situ* formation of carbamic acid within the MOF structure. Our approach is unique in leveraging the internal pore chemistry to enhance CO_2 capture, demonstrating that the incorporation of a Lewis basic species within a MOF can significantly amplify its CO_2 adsorption capacity.

RESULTS AND DISCUSSION

Synthesis and Characterization

The MOF employed in our study is a copper paddlewheel-based MOF known as *m***CBMOF-1**, with the chemical formula $[Cu_2(m\text{CB-L})_2(\text{DABCO})_{0.5}(H_2O)]\cdot$guest molecules, in which *m*CB-L refers to 1,7-di(4-carboxyphenyl)-1,7-dicarba-*closo*-dodecaborane and DABCO represents 1,4-diazabicyclo[2.2.2]-octane (Figure 1).[50,51] The synthesis of *m***CBMOF-1** is carried out in a mixture of water, ethanol, and dimethylformamide (DMF) (in a ratio of 1:5:5) at 80 °C for 48 h. Powder X-ray diffraction (PXRD, Figure 2a) was utilized to verify the identity and purity of the material, while Fourier transform infrared (FTIR) spectra (Figure S1) confirmed the successful incorporation of the ligands into the MOF structure. The MOF crystallizes in tetragonal space group *I*422, and the atomic coordinates allow for the following chemical interpretation of the structure. The *m*CB ligands, which feature a chevron shape with an opening angle of 117°, are linked by Cu_2 paddlewheels, forming a 4^4 net (**sql**). The top and the bottom of this two-dimensional layer are decorated with aqua and DABCO ligands, which complete the coordination sphere of Cu_2 paddlewheels. The DABCO ligands connect the two-dimensional layer to neighboring ones, and two such layers are related to each other by a 2_1-axis (rotation by 180° followed by translation by $b/2$). Because DABCO ligands are present on both sides of each two-dimensional layer, they extend the coordination to a three-dimensional $4^4{\cdot}6^6$ net (**sqp**). The structure of *m***CBMOF-1** consists of two interpenetrating nets, which collectively occupy

https://doi.org/10.1021/jacsau.4c00808
JACS Au 2024, 4, 4833−4843

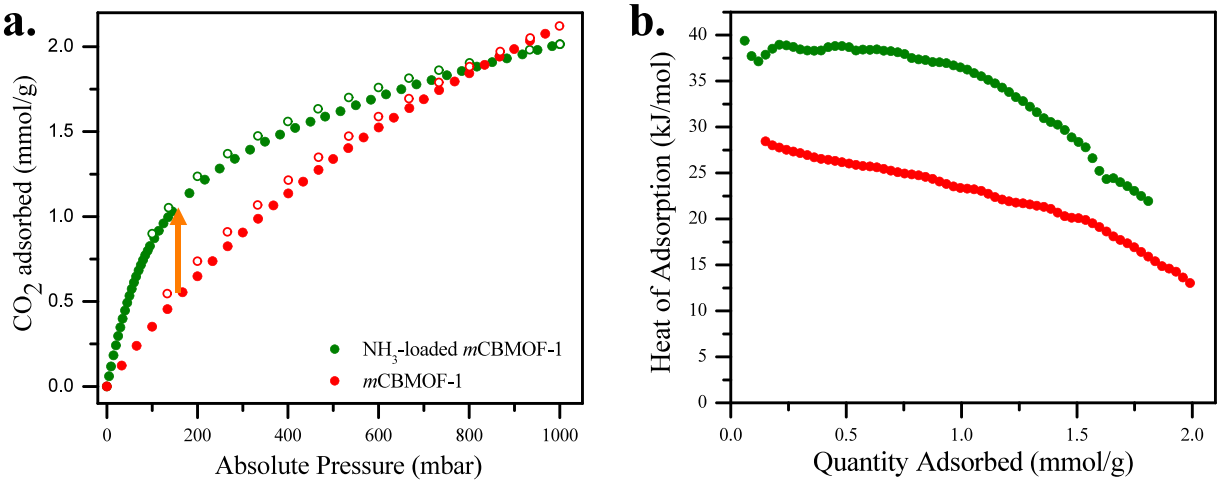

Figure 3. Carbon dioxide uptake and isosteric heat of adsorption. (a) Comparison of the CO_2 isotherms for activated ***m*CBMOF-1** (shown in red) and NH_3-loaded (shown in green) at 298 K. At 150 mbar (orange arrow), the NH_3-loaded (∼1 mmol/g) ***m*CBMOF-1** exhibited 106% higher CO_2 uptake compared to that of ***m*CBMOF-1**. (b) Isosteric heat of CO_2 adsorption calculated for the activated (red) and NH_3-loaded (green) ***m*CBMOF-1.**.

67.6% of the unit-cell volume, leaving 32.4% as void space, as determined by the Void routine of the Olex2 crystallographic software.[52] The void system comprises one-dimensional channels running along [110], interconnected along [001] by narrow segments (Figure 1d). Removal of aqua ligands from the crystal structure increases the void volume to 34.5% and generates an additional channel along [001] (Figure 1e, Figure S2), which is potentially accessible for gas diffusion. The channel is lined with four Cu(II) open metal sites situated at the vertices of a square, with a distance of 6.042 Å between the adjacent Cu(II) atoms and 8.545 Å between opposite ones (Figure S3). This four-Cu_2 site plays a key role in the adsorption properties of ***m*CBMOF-1** (see below).

Thermogravimetric analysis (TGA) of ***m*CBMOF-1** shows a 19% weight loss attributed to the removal of solvent molecules (water, DMF) present in the voids of the ***m*CBMOF-1** (Figure S4). The thermal activation of ***m*CBMOF-1** induces a color change from sky blue to deep navy (Figure S5), which is consistent with the removal of coordinated water molecules and the presence of open Cu^{2+} sites.[53] When the activated ***m*CBMOF-1** is exposed to air, it returns to its original sky-blue color due to the recoordination of water molecules present in air to active Cu^{2+} centers. This phenomenon is in line with observations seen in other Cu(II)-based MOFs such as HKUST-1[54,55] and Cu-MOF-2.[53] Furthermore, the ultraviolet−visible (UV−vis) spectrum of ***m*CBMOF-1** exhibits an absorption peak with a λ_{max} of 744 nm (Figure S6). This absorption peak corresponds to the *d*−*d* electronic transition in Cu^{2+} and gives the material a sky-blue color.

Upon exposure of the activated ***m*CBMOF-1** to gaseous NH_3 at 1 bar for >2 h, it undergoes a color change to dark purple (Figure S7), and its UV−vis spectrum displays an absorption peak at λ_{max} of 647 nm (Figure S6). These changes in the optical properties arise from the coordination of NH_3 to open Cu(II) sites and the positioning of NH_3 in the spectrochemical series. A comparison with the pristine ***m*CBMOF-1** (λ_{max} = 744 nm) provides valuable insights: given that H_2O is a weak field ligand and NH_3 is a strong field ligand, the energy required for the *d*−*d* transition in an amine complex is higher compared to the aqua complex.[56] The PXRD pattern of NH_3-loaded ***m*CBMOF-1** (Figure S8) reveals that the MOF becomes amorphous, indicating that the metal−ligand bonds in the MOF are disrupted. FTIR spectroscopy shows an additional peak at 3320 cm^{-1}, corresponding to N−H stretching in the bound NH_3 molecule (Figures S2 and S9). When ***m*CBMOF-1** was exposed to a low NH_3 concentration (∼1 mmol/g loading), its PXRD pattern remained crystalline. The TGA profile of this material is comparable to that of the as-made MOF (Figure S4), indicating that NH_3 loading and binding to Cu sites do not affect the material's stability. Furthermore, ^1H and ^{13}C solution NMR in DMSO-d_6 of the controlled (∼1 mmol/g) NH_3-loaded ***m*CBMOF-1** demonstrates the stability of the MOF with no leaching of the *m*CB ligand in the solution (Figures S10 and S11).

Adsorption Properties

At 77 K and 1 bar, activated ***m*CBMOF-1** adsorbs N_2, as indicated by its type I adsorption isotherm (Figure 2b, Figure S12a), with a BET surface area of 996 m^2/g. The single point adsorption total pore volume at p/p^0 = 0.90 is 0.516 cm^3/g, which is consistent with 0.632 cm^3/g derived from the static crystal structure of ***m*CBMOF-1** (refined against data collected at 100 K). The activated ***m*CBMOF-1** displays a low affinity for CO_2, evident from the quasi-linear shape of its adsorption isotherm (Figure 2c) and a relatively low isosteric heat of CO_2 adsorption (Q_{st}) of 28 kJ/mol (Figure 3b). This Q_{st} value positions ***m*CBMOF-1** among the MOFs with moderate performance toward CO_2 capture such as HKUST-1 (Q_{st} = 24−28 kJ/mol),[30,57] UiO-66 (Q_{st} = 26 kJ/mol),[29] and MIL-100(Fe) (Q_{st} = 30 kJ/mol)[57] but falls behind Mg-MOF-74 (Q_{st} = 47 kJ/mol) with its open metal sites.[27]

To investigate the NH_3 adsorption properties of ***m*CBMOF-1**, NH_3 isotherms were recorded (Figure 2d). Pure (99.995%) NH_3 isotherms collected at 298 K and 1 bar demonstrated that 1 g of activated ***m*CBMOF-1** uptakes 11.5 mmol of NH_3. This uptake corresponds to 43.6 molecules of NH_3 per unit cell (Figure 2d), a quantity comparable to what is observed in other MOFs featuring open metal sites, suggesting a strong affinity for NH_3.[58−63] This remarkable uptake can be explained by two consecutive phenomena. At low pressures, NH_3 (Lewis base) forms coordination bonds with open Cu sites (Lewis acid), allowing a maximum of four NH_3 molecules to bind in one unit cell of activated ***m*CBMOF-1**. As the pressure

https://doi.org/10.1021/jacsau.4c00808
JACS Au 2024, 4, 4833−4843

increases, NH_3 fills the pores through dispersive interactions and H-bonds. The high affinity of activated ***m*CBMOF-1** for NH_3 is further supported by the hysteresis observed in its isotherm (Figure 2d) and the density functional theory- (DFT-) calculated energy of −119.8 kJ/mol for the preferred NH_3 adsorption site (Figure S13). The high value of adsorption energy indicates that NH_3 undergoes chemical bonding within the MOF, implying that the unsaturated Cu sites act as the primary adsorption sites.[60] Additionally, the desorption curves reveal that initially only a small amount of NH_3 is released, and even as the pressure decreases to zero, a substantial amount of NH_3 remains in the MOF structure and pores. During the second isotherm, the hysteresis observed in the NH_3 isotherm at 298 K indicates a maximum uptake of ***m*CBMOF-1** at 5.9 mmol/g (22.5 molecules/unit cell; Figure 2d). The lower NH_3 uptake during the second NH_3 isotherm is likely attributed to some NH_3 molecules being strongly bound to its active sites during the first cycle. However, the BET surface area of the NH_3-loaded ***m*CBMOF-1** is 6 m^2/g, suggesting that NH_3 molecules disrupt its long-range order, and it becomes nonporous to N_2 at 77 K and 1 bar (Figure S12b). When the amorphous NH_3-loaded material is immersed in water, the resulting material becomes crystalline (Figure S8). This material is likely to be a new structure, as the Bragg reflections do not match those of ***m*CBMOF-1**, and is porous to N_2 at 77 K (Figure S12c). Efforts to elucidate the structure of this new phase through single-crystal X-ray diffraction have been unsuccessful due to the polycrystalline nature of the material. Saturating ***m*CBMOF-1** with NH_3 renders it nonporous to N_2 at 77 K, as NH_3 molecules occupy both the Cu(II) coordination sites and all the pores. To prevent this, we exposed the activated ***m*CBMOF-1** to a controlled amount of NH_3 gas, thereby achieving an uptake of ∼1.0 mmol/g, equivalent to one NH_3 molecule binding to one open Cu site. The resulting material (∼1.0 $mmol_{NH3}/g$ loading) was porous to N_2 at 77 K and 1 bar, and its BET surface area was 686 m^2/g (Figure S12d). The BET surface area of NH_3-loaded (∼1.0 mmol/g) ***m*CBMOF-1** is lower than the activated ***m*CBMOF-1**, likely due to a partial loss of crystallinity and/or occupation of the pores with NH_3. Interestingly, controlled ammonia-loaded (∼1 mmol/g) ***m*CBMOF-1** does not collapse and can be fully regenerated upon immersion in water, as confirmed by PXRD (Figure S14a). The BET surface area of regenerated ***m*CBMOF-1** is 923 m^2/g (Figure S14b). Its regeneration is thought to be due to the recoordination of water molecules to the $4Cu_2$ sites, displacing NH_3 molecules from the MOF structure.[56] These observations confirm the stability of ***m*CBMOF-1** when it is loaded with ∼1 mmol/g of NH_3. Elemental analysis of the NH_3-loaded (∼1 mmol/g) ***m*CBMOF-1** indicated the presence of 1.9 molecules of NH_3 per formula unit, $[Cu_2(m\text{CB-L})_2(\text{DABCO})_{0.5}(NH_3)_{1.9-x}]\cdot x NH_3\cdot 0.3H_2O$ (Table S1), some of which are coordinated to the open Cu centers of ***m*CBMOF-1**.[64] Overrepresentation of the NH_3 molecules in this formula may stem from the inherent imprecision of CHN analysis.

Mechanism of CO_2 Adsorption

The ***m*CBMOF-1** loaded with a controlled amount of adsorbed NH_3 was further investigated toward CO_2 capture. As shown in Figure 3a and Figures S15 and S16, the material features type I bent-shaped CO_2 adsorption isotherms, a distinctive feature evident when compared to the CO_2 isotherm of activated ***m*CBMOF-1** (Figure 2c). The consistency in the shape of the CO_2 isotherms was verified across three distinct experiments (Figure S16), emphasizing the reliability and reproducibility of our findings. At 150 mbar and 298 K, conditions relevant to postcombustion carbon capture, the activated MOF exhibited a CO_2 uptake of 0.51 mmol/g. However, after doping activated ***m*CBMOF-1** with a controlled amount of gaseous NH_3, the uptake at the same pressure and temperature increased to 1.05 mmol/g (Figure 3a). A similar increase was observed in Q_{st} at low coverage, which was 28 kJ/mol for the activated MOF and increased to 39 kJ/mol for the NH_3-loaded ***m*CBMOF-1** (Figure 3b). These findings indicate different CO_2 adsorption mechanisms in the two discussed materials. The enhanced adsorption can be attributed to the synergy of acid−base interactions and hydrogen bonding of CO_2 and the NH_3 groups bound to the MOF pores through the open metal sites.[40,65−68] The CO_2 isotherm of the NH_3-loaded ***m*CBMOF-1** does not exhibit an adsorption hysteresis, a characteristic that has not been detected in other chemisorption-based materials as well.[49,69]

FTIR and solid-state NMR techniques were employed to investigate the interactions between CO_2 and NH_3 within the pores of ***m*CBMOF-1**. In the FTIR spectra, new peaks emerged at 3300 and 480 cm^{-1} upon NH_3 loading into the activated MOF, corresponding to N−H and Cu−N stretching frequencies,[70] respectively (Figure S9). In the NH_3−CO_2 loaded ***m*CBMOF-1**, the appearance of additional peaks at 3366 and 1633 cm^{-1} indicates coordinated NH_3 vibrations,[71−73] suggesting the possible formation of carbamic acid upon sequential introduction of NH_3 and CO_2 into the pores of ***m*CBMOF-1**.

Solid-state ^{13}C NMR was employed to investigate the structural modification occurring upon the introduction of NH_3 and subsequent CO_2 loading in the paramagnetic ***m*CBMOF-1**.[74−76] This method was adapted to explore the binding of NH_3 and CO_2 in ***m*CBMOF-1**. Figure 4 illustrates the ^{13}C solid-state NMR spectra for the as-made and NH_3-CO_2 loaded m**CBMOF-1.** In the spectrum of the as-made ***m*CBMOF-1** (Figure 4a), the resonances observed at 31.1, 34.6, and 164.0 ppm are attributed to the carbon atoms of the guest dimethylformamide (DMF) molecules located within the MOF pores. The resonance at 49.6 ppm corresponds to the carbon atom of the *m*-carborane group, while the peaks within the range of 132 to 150 ppm represent the aromatic C of the benzoate fragment of the *m*CB ligand. Additionally, the peak at 173.3 ppm corresponds to carbonyl C of the carboxylate group of the ligand. The resonance at 79.7 ppm indicates a single environment for the carbon atoms in the coordinated DABCO. This resonance is shifted to the downfield region due to paramagnetic shift, compared to the free DABCO molecule, which appears at 47.9 ppm (Figure S17). Some aspects of the NMR spectra present paramagnetic shifts that are the subject of further study. The ss-NMR of the activated MOF shows that the peaks at 31.1, 34.6, and 164 ppm are absent, confirming the removal of DMF molecules from the pores of the MOF (Figure S18a). All other peaks in the as-made MOF remain in the activated MOF, confirming its structural stability. The successful loading of NH_3 in activated ***m*CBMOF-1** is evidenced by two distinct resonances at 79.7 and 72.0 ppm for the DABCO ligand in the MOF structure. These resonances suggest two distinct environments for the carbon in DABCO: DABCO−Cu-dimer−NH_3 and DABCO−Cu-dimer−open Cu site (Figure S18b). The broadened resonance at 169.9 ppm, corresponding to the carboxylic carbon of the

https://doi.org/10.1021/jacsau.4c00808
JACS Au 2024, 4, 4833−4843

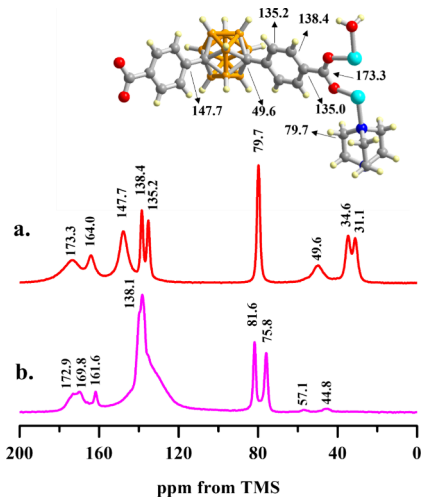

Figure 4. Solid-state ^{13}C NMR spectra for (a) as-made ***m*CBMOF-1** (inset: a fraction of ***m*CBMOF-1** and corresponding assignments for its individual carbon atoms). The resonances at 31.1, 34.6, and 164.0 ppm correspond to the guest DMF molecules encapsulated within the MOF pores. (b) CO_2 loading on the NH_3-functionalized ***m*CBMOF-1**. The resonances corresponding to DMF are absent, confirming its successful activation followed by NH_3 and CO_2 loading. The resonance at 161.6 ppm corresponds to the carbonyl carbon of carbamic acid, indicating that CO_2 is chemisorbed upon loading on the NH_3-loaded ***m*CBMOF-1**.

*m*CB ligand, can be attributed to a dynamic environment around the Cu-dimer in NH_3-loaded ***m*CBMOF-1**. Other peaks closely match the position and intensity of those in activated ***m*CBMOF-1**, underscoring the chemical similarity of the two materials.

The successful loading of CO_2 in the NH_3 loaded ***m*CBMOF-1** is evident from the more distinct peaks in the ^{13}C NMR spectrum compared to those of the as-made MOF (Figure 4b, Figure S18c). In the NH_3-CO_2 loaded MOF, the resonances at 81.6 and 75.8 ppm are attributed to DABCO. The presence of multiple resonances for DABCO carbon atoms indicates the emergence of distinct chemical environments within DABCO. Given that DABCO is bound to one side of the Cu(II) paddlewheels, occupying the opposite coordination site can change the electronic structure of Cu(II) paddlewheels, as evidenced by the chemical shifts of DABCO. Importantly, the presence of two nonequivalent sites, which are not equally populated, suggests that only a portion of Cu sites are coordinated with the NH_3 molecules. This is further supported by the observed peak splitting at 44.8 and 57.1 ppm, which is thought to be due to the distortion of the *m*CB ligand in the MOF structure. Our findings are consistent with our elemental analysis revealing that each formula unit of ***m*CBMOF-1** hosts 1.9 molecules of NH_3 (chemisorbed and/or physisorbed). This observation has significant implications for our DFT results described below. The resonances at 172.9 and 169.8 ppm corresponding to carboxylic carbon of the *m*CB ligand can be attributed to a dynamic environment around the Cu(II) paddlewheels in the NH_3-CO_2 loaded ***m*CBMOF-1**.[74] The resonances ranging from 122 to 150 ppm correspond to the aromatic carbons of the *m*CB ligand, while the peak at 44.8

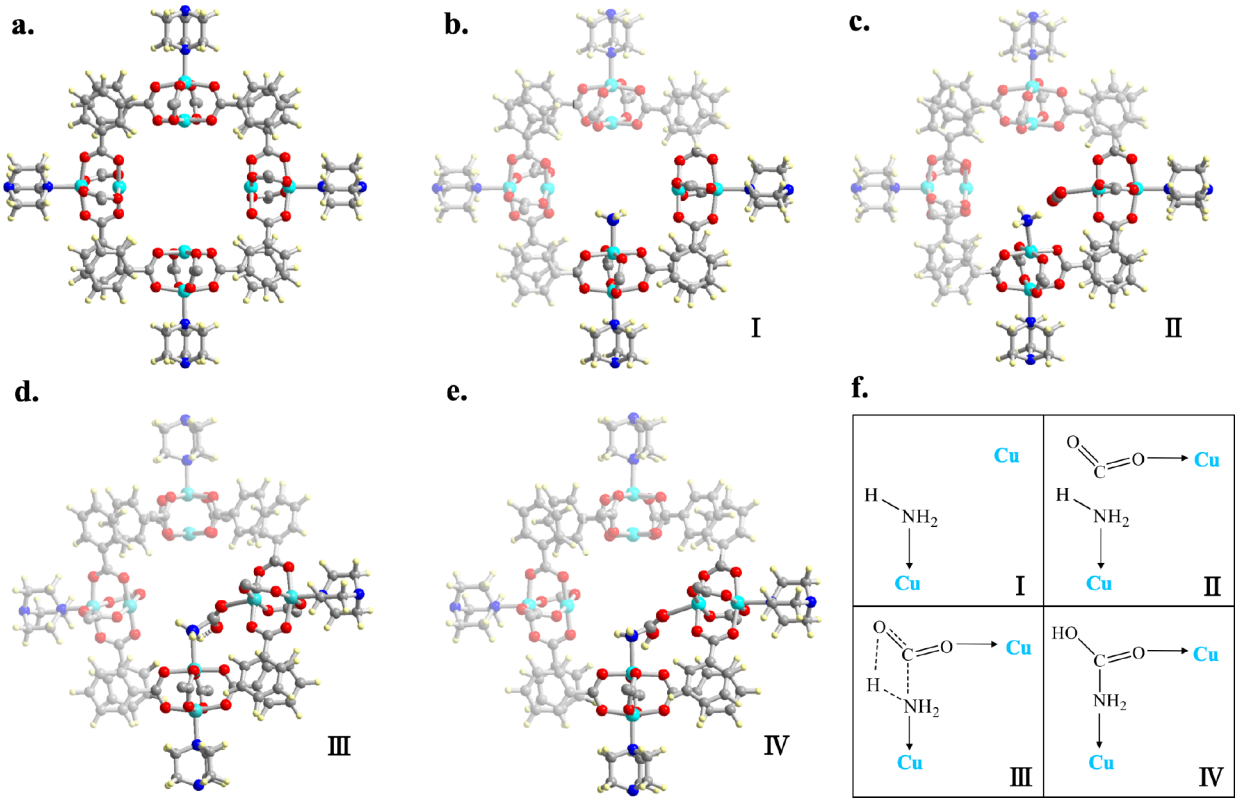

Figure 5. Mechanistic overview of the CO_2 capture with ***m*CBMOF-1**. DFT optimized configurations of (a) activated ***m*CBMOF-1**, (b) NH_3 absorbed in activated ***m*CBMOF-1**, (c) CO_2 adsorbed in NH_3-loaded ***m*CBMOF-1**, (d) transition state of CO_2 interacting with NH_3 within the pore of ***m*CBMOF-1**, (e) product of the CO_2 + NH_3 reaction within the pore of ***m*CBMOF-1**, and (f) a schematic illustration of the carbamic acid formation pathway, steps I–IV. Atom color code: gray for C, red for O, blue for N, sky blue for Cu and pale yellow for H.

https://doi.org/10.1021/jacsau.4c00808
JACS Au 2024, 4, 4833–4843

ppm corresponds to *m*-C of the carborane core in the ligand. In line with the literature, the peak at 161.6 ppm corresponds to carbon in carbamic acid ($H_2N-COOH$).[47,49,77,78] This peak differs significantly from the carbon peak at 166.1 ppm in ammonium carbamate (Figure S19), suggesting the formation of carbamic acid within the pores of our MOF.

The DFT sheds light on the interactions between Cu(II)-paddlewheels and CO_2 or NH_3 via isosurface plots of charge differences (Figure S20) and the formation of carbamic acid within the pores of the MOF structure (Figure 5). For the coadsorption intermediate state, the NH_3 molecule is adsorbed on an open Cu(II) site (Figure 5b,f(I)), while CO_2 molecules interact with the adjacent open Cu(II) site (Figure 5c,f(II)). The coadsorbed CO_2 and NH_3 molecules further interact with each other to generate a motif ($Cu(II)-NH_3-CO_2$), which is an exothermic step with the calculated reaction energy of −15.2 kJ/mol (Figure 5d,f(III) and Figure S13). At the transition state (TS), the H atom of NH_3 approaches the O atom of the CO_2, forming the O═C---N−H intermediate. The calculated energy of activation is 18.8 kJ/mol, indicating that the formation of $-NH_2COOH$ is kinetically feasible (Figure 5e,f(IV)) with a further energy release of 23.8 kJ/mol. These results clearly indicate that the presence of the coordinated NH_3 molecule, anchored in the unique environment of four open Cu(II) sites located in proximity to one another, significantly improves the immobilization of CO_2. This enhancement results in the formation of the $Cu(II)-NH_3-CO_2$ intermediate followed by the stable $Cu(II)-NH_2COOH$ complex within the pores of ***m*CBMOF-1**.

The pathway described in our work for the formation of carbamic acid differs significantly from the mechanism reported with Mg_2-(dobpdc) and diamines.[49,79−81] Mg_2-(dobpdc) is a mesoporous MOF with a pore size of 22 Å having six Mg(II) open metal sites in the pore.[82] When diamine is introduced into the MOF, it interacts with the metal in the pore, forming coordination bonds. Subsequently, CO_2 is cooperatively inserted into the Mg−N bond, forming a carbamate in dry conditions and carbamic acid if water is present.[47,81] The landscape in our microporous ***m*CBMOF-1** is unique, and both NH_3 and CO_2 coordinate to metal centers first and then, due to the proximity of those centers, react to form carbamic acid (Figure 5f).

CONCLUSIONS

Our study reports, for the first time, that sequential pore functionalization in a MOF with open Cu(II) sites leads to a 106% enhancement of CO_2 adsorption at low pressures. The activated ***m*CBMOF-1** comprises repeating units with four active open Cu(II) sites positioned in proximity to one another on vertices of a square cross section of the pore; upon exposure to NH_3, some of these Cu(II) sites, acting as a Lewis acid, interact with molecules of NH_3, a Lewis base, through coordination bonding. The remaining open Cu(II) sites are available for subsequent CO_2 coordination. When both CO_2 and NH_3 are anchored in the unique coordination environment of the pore, they interact with each other, forming a carbamic acid species, as inferred from our FTIR, ^{13}C solid-state NMR, and DFT results. This interaction is evident as NH_3-functionalized pores attract CO_2 more strongly than the nonfunctionalized activated ***m*CBMOF-1**: the CO_2 uptake at 150 mbar and 298 K increases by 106%, and Q_{st} increases by 40%. Discovering MOFs with unique pores geometries and active sites and applying postsynthetic functionalization could pave the way for further advancements in CO_2 capture from dilute sources.

EXPERIMENTAL SECTION

Materials

All the materials and chemicals used in this study were bought from commercial sources such as MilliporeSigma, Sigma-Aldrich, and Tokyo Chemical Industry and used without further purification.

Synthesis of mCB-H_2L

1,7-Di(4-carboxyphenyl)-1,7-dicarba-*closo*-dodecaborane ligand (*m*CB-H_2L) was synthesized as per the literature procedure.[50]

Synthesis of *m*CBMOF-1 [$(Cu_2(mCB\text{-}L)_2(DABCO)_{0.5}(H_2O))\cdot 2DMF\cdot 2H_2O$]

***m*CBMOF-1** was synthesized as per the reported procedure.[50] Briefly, DABCO (6.5 mg, 0.059 mmol), *m*CB-H_2L (90 mg, 0.234 mmol), H_2O (1 mL), and DMF (5 mL) were mixed in an 8 dram vial, and the mixture was sonicated until all the solids were dissolved. Next, $Cu(NO_3)_2\cdot 6H_2O$ (68 mg, 0.234 mmol) was added in ethanol (5 mL) and sonicated until the metal salt was completely dissolved. The two solutions were mixed and heated at 80 °C for 48 h to obtain green crystals. Finally, the crystals were washed with DMF and acetone and dried at 80 °C to obtain ***m*CBMOF-1**.

Activation of *m*CBMOF-1

A sample of ***m*CBMOF-1** was enclosed in a Schlenk tube and heated under a vacuum for 24 h at 120 °C using an oil bath to remove water molecules from the pores.

Loading *m*CBMOF-1 with Excess NH_3

Ammonia loading was conducted using either the 3FLEX gas analyzer from Micromeritics or the Schlenk methods. In the Schlenk method, the knob of the tube containing activated ***m*CBMOF-1** was charged with pure ammonia gas (utilizing a pressure gauge) at 1 bar for ∼1 h, sealed, and allowed to equilibrate for an additional ∼1 h.

Regeneration of *m*CBMOF-1 after Ammonia Loading

Ammonia loaded MOF was soaked in water for 15 min with stirring. After that, it was washed with water followed by acetone and dried at 80 °C.

Loading *m*CBMOF-1 with a Controlled Amount of NH_3

Pristine ***m*CBMOF-1** was introduced into a borosilicate glass tube and activated under a vacuum for 24 h at 120 °C. A set amount adsorbed of ∼1.00 $mmol_{NH3}/g$ was achieved with a 3FLEX Adsorption Analyzer.

Loading the NH_3-loaded *m*CBMOF-1 with CO_2

***m*CBMOF-1** loaded with ∼1.00 $mmol_{NH3}/g$ was transferred to a Parr reactor, which was then filled with CO_2 gas to 1 bar at room temperature and ∼1 h to achieve equilibrium.

ASSOCIATED CONTENT

Data Availability Statement

The data that support the findings of the study are included in the main text and the Supporting Information file. Raw data can be obtained from the corresponding author upon request. Solid-state NMR raw data collected from 400 MHz have been deposited on Dryad at https://doi.org/10.5061/dryad.v15dv426b.[83]

Supporting Information

The Supporting Information is available free of charge at https://pubs.acs.org/doi/10.1021/jacsau.4c00808.

Detailed characterization methods (PXRDs, TGA, FTIR, gas sorption, ss-NMR, dynamic CO_2 capture), characterization data, and computational studies (PDF)

https://doi.org/10.1021/jacsau.4c00808
JACS Au 2024, 4, 4833−4843

AUTHOR INFORMATION

Corresponding Authors

Hongliang Huang − *State Key Laboratory of Separation Membranes and Membrane Processes, School of Chemistry and Chemical Engineering, Tiangong University, Tianjin 300387, China;* orcid.org/0000-0001-9690-9259; Email: huanghongliang@tiangong.edu.cn

Kyriakos C. Stylianou − *Materials Discovery Laboratory (MaD Lab), Department of Chemistry, Oregon State University, Corvallis, Oregon 97331, United States;* orcid.org/0000-0003-1670-0020; Email: kyriakos.stylianou@oregonstate.edu

Authors

Ankit K. Yadav − *Materials Discovery Laboratory (MaD Lab), Department of Chemistry, Oregon State University, Corvallis, Oregon 97331, United States*

Andrzej Gładysiak − *Materials Discovery Laboratory (MaD Lab), Department of Chemistry, Oregon State University, Corvallis, Oregon 97331, United States;* orcid.org/0000-0003-3302-1644

Ah-Young Song − *Department of Chemical and Biomolecular Engineering, University of California, Berkeley 94720, United States*

Lei Gan − *Institut de Ciència de Materials de Barcelona (ICMAB-CSIC), Bellaterra 08193, Spain; School of Chemistry and Materials Science, Nanjing Normal University, Nanjing 210023, P. R. China*

Casey R. Simons − *Center for Advanced Materials Characterization in Oregon, University of Oregon, Eugene, Oregon 97403, United States;* orcid.org/0000-0002-8024-6996

Nawal M. Alghoraibi − *ARAMCO, Dhahran 31311, Saudi Arabia*

Ammar H. Alahmed − *ARAMCO, Dhahran 31311, Saudi Arabia*

Mourad Younes − *ARAMCO, Dhahran 31311, Saudi Arabia*

Jeffrey A. Reimer − *Department of Chemical and Biomolecular Engineering, University of California, Berkeley 94720, United States*

José G. Planas − *Institut de Ciència de Materials de Barcelona (ICMAB-CSIC), Bellaterra 08193, Spain;* orcid.org/0000-0002-1648-2169

Complete contact information is available at: https://pubs.acs.org/10.1021/jacsau.4c00808

Author Contributions

CRediT: **Ankit Yadav** conceptualization, formal analysis, investigation, methodology, visualization, writing - original draft; **Andrzej Gładysiak** conceptualization, formal analysis, investigation, methodology, visualization, writing - original draft; **Ah-Young Song** formal analysis, investigation, methodology, writing - review & editing; **Lei Gan** investigation, writing - review & editing; **Casey Simons** investigation, writing - review & editing; **Nawal M. Alghoraibi** methodology, writing - review & editing; **Ammar H. Alahmed** methodology, writing - review & editing; **Mourad Younes** methodology, writing - review & editing; **Jeffrey A. Reimer** conceptualization, funding acquisition, methodology, supervision, writing - review & editing; **Hongliang Huang** conceptualization, funding acquisition, investigation, supervision, writing - review & editing; **Jose Giner Planas** conceptualization, funding acquisition, methodology, supervision, writing - review & editing; **Kyriakos C. Stylianou** conceptualization, funding acquisition, investigation, methodology, supervision, visualization, writing - original draft.

Notes

The authors declare no competing financial interest.

ACKNOWLEDGMENTS

K.C.S., A.G., and A.K.Y. thank Dr. Patrick Reardon for assistance with the NMR experiments. MaD Lab thanks Marilyn and Brian Kleiner for their generous support of this project through their donor advised fund. K.C.S. acknowledges support from Saudi Aramco for the development of this project and thanks Dr. Aqil Jamal for useful discussions. K.C.S. thanks the Department of Chemistry at Oregon State University (OSU) for support through start-up funding and College of Science Industrial Partnership Award. A.K.Y. acknowledges support from the Department of Chemistry for the Milton Harris fellowship (2023). K.C.S. thanks Baydin Inc., maker of the Boomerang productivity suite, for supporting this work. J.G.P. thanks Spanish Ministerio de Ciencia e Innovación project PID2022-136892NB-I00 and the Generalitat de Catalunya (2021/SGR/00442) for financial support. A.S. gratefully acknowledges support as a Pines Magnetic Resonance Center Postdoctoral Fellow. We thank Drs. Hasan Celik, Raynald Giovine, and UC Berkeley's NMR facility in the College of Chemistry (CoC-NMR) for spectroscopic assistance. The instrument used in this work is supported by the National Science Foundation under Grant No. 2018784.

REFERENCES

(1) Lashof, D. A.; Ahuja, D. R. Relative contributions of greenhouse gas emissions to global warming. *Nature* **1990**, *344* (6266), 529−531.

(2) Herzog, H.; Eliasson, B.; Kaarstad, O. Capturing Greenhouse Gases. *Sci. Am.* **2000**, *282* (2), 72−79.

(3) Zhong, W.; Haigh, J. D. The greenhouse effect and carbon dioxide. *Weather* **2013**, *68* (4), 100−105.

(4) Plass, G. N. Carbon Dioxide and Climate. *Sci. Am.* **1959**, *201* (1), 41−47.

(5) Karl, T. R.; Trenberth, K. E. Modern Global Climate Change. *Science* **2003**, *302* (5651), 1719−1723.

(6) Liu, T.; Luo, D.; Xu, D.; Zeng, H.; Lin, Z. Solvent induced structural variation in magnesium carboxylate frameworks. *Inor. Chem. Commun.* **2013**, *29*, 110−113.

(7) Hofmann, D. J.; Butler, J. H.; Tans, P. P. A New Look at Atmospheric Carbon Dioxide. *Atmos. Environ.* **2009**, *43* (12), 2084−2086.

(8) Hashimoto, K., Global Temperature and Atmospheric Carbon Dioxide Concentration. In *Global Carbon Dioxide Recycling: For Global Sustainable Development by Renewable Energy*, Hashimoto, K., Ed. Springer: Singapore, 2019; pp 5−17.

(9) Rockström, J.; Steffen, W.; Noone, K.; Persson, Å.; Chapin, F. S.; Lambin, E. F.; Lenton, T. M.; Scheffer, M.; Folke, C.; Schellnhuber, H. J.; Nykvist, B.; de Wit, C. A.; Hughes, T.; van der Leeuw, S.; Rodhe, H.; Sörlin, S.; Snyder, P. K.; Costanza, R.; Svedin, U.; Falkenmark, M.; Karlberg, L.; Corell, R. W.; Fabry, V. J.; Hansen, J.; Walker, B.; Liverman, D.; Richardson, K.; Crutzen, P.; Foley, J. A. A safe operating space for humanity. *Nature* **2009**, *461* (7263), 472−475.

(10) Hansen, J.; Sato, M.; Kharecha, P.; Beerling, D.; Berner, R.; Masson-Delmotte, V.; Pagani, M.; Raymo, M.; Royer, D. L.; Zachos, J. C. Target Atmospheric CO_2: Where should Humanity Aim? *Open Atmos. Sci. J.* **2008**, *2*, 217.

(11) Nandi, S.; De Luna, P.; Daff, T. D.; Rother, J.; Liu, M.; Buchanan, W.; Hawari, A. I.; Woo, T. K.; Vaidhyanathan, R. A Single-ligand Ultra-microporous MOF for Precombustion CO_2 Capture and Hydrogen Purification. *Sci. Adv.* **2015**, *1* (11), No. e1500421.
(12) Ahmed, S. A.; Diffenbaugh, N. S.; Hertel, T. W. Climate Volatility Deepens Poverty Vulnerability in Developing Countries. *Environ. Res. Lett.* **2009**, *4* (3), No. 034004.
(13) Awaworyi Churchill, S.; Smyth, R.; Trinh, T.-A. Energy Poverty, Temperature and Climate Change. *Energy Econ.* **2022**, *114*, No. 106306.
(14) Falcaro, P.; Ricco, R.; Doherty, C. M.; Liang, K.; Hill, A. J.; Styles, M. J. MOF Positioning Technology and Device Fabrication. *Chem. Soc. Rev.* **2014**, *43* (16), 5513−5560.
(15) Eddaoudi, M.; Sava, D. F.; Eubank, J. F.; Adil, K.; Guillerm, V. Zeolite-like Metal−organic Frameworks (ZMOFs): Design, Synthesis, and Properties. *Chem. Soc. Rev.* **2015**, *44* (1), 228−249.
(16) Mandal, S.; Natarajan, S.; Mani, P.; Pankajakshan, A. Post-Synthetic Modification of Metal−organic Frameworks Toward Applications. *Adv. Funct. Mater.* **2021**, *31* (4), No. 2006291.
(17) Rowsell, J. L. C.; Yaghi, O. M. Metal−organic Frameworks: A New Class of Porous Materials. *Microporous Mesoporous Mater.* **2004**, *73* (1), 3−14.
(18) Zhang, X.; Chen, Z.; Liu, X.; Hanna, S. L.; Wang, X.; Taheri-Ledari, R.; Maleki, A.; Li, P.; Farha, O. K. A Historical Overview of the Activation and Porosity of Metal−organic Frameworks. *Chem. Soc. Rev.* **2020**, *49* (20), 7406−7427.
(19) Xiang, S.; He, Y.; Zhang, Z.; Wu, H.; Zhou, W.; Krishna, R.; Chen, B. Microporous Metal-organic Framework with Potential for Carbon Dioxide Capture at Ambient Conditions. *Nat. Commun.* **2012**, *3* (1), 954.
(20) Sumida, K.; Rogow, D. L.; Mason, J. A.; McDonald, T. M.; Bloch, E. D.; Herm, Z. R.; Bae, T.-H.; Long, J. R. Carbon Dioxide Capture in Metal−organic Frameworks. *Chem. Rev.* **2012**, *112* (2), 724−781.
(21) Piscopo, C. G.; Loebbecke, S. Strategies to Enhance Carbon Dioxide Capture in Metal-Organic Frameworks. *ChemPlusChem.* **2020**, *85* (3), 538−547.
(22) Chiu, N. C.; Loughran, R. P.; Gładysiak, A.; Vismara, R.; Park, A.-H. A.; Stylianou, K. C. Wet flue gas CO_2 capture and utilization using one-dimensional metal−organic chains. *Nanoscale* **2022**, *14* (40), 14962−14969.
(23) Liang, W.; Bhatt, P. M.; Shkurenko, A.; Adil, K.; Mouchaham, G.; Aggarwal, H.; Mallick, A.; Jamal, A.; Belmabkhout, Y.; Eddaoudi, M. A Tailor-Made Interpenetrated MOF with Exceptional Carbon-Capture Performance from Flue Gas. *Chem.* **2019**, *5* (4), 950−963.
(24) Zhou, S.; Shekhah, O.; Jin, T.; Jia, J.; Datta, S. J.; Bhatt, P. M.; Eddaoudi, M. A CO_2-recognition metal-organic framework membrane for continuous carbon capture. *Chem.* **2023**, *9* (5), 1182−1194.
(25) Lin, J.-B.; Nguyen, T. T. T.; Vaidhyanathan, R.; Burner, J.; Taylor, J. M.; Durekova, H.; Akhtar, F.; Mah, R. K.; Ghaffari-Nik, O.; Marx, S.; Fylstra, N.; Iremonger, S. S.; Dawson, K. W.; Sarkar, P.; Hovington, P.; Rajendran, A.; Woo, T. K.; Shimizu, G. K. H. A scalable metal-organic framework as a durable physisorbent for carbon dioxide capture. *Science* **2021**, *374* (6574), 1464−1469.
(26) Loughran, R. P.; Hurley, T.; Gładysiak, A.; Chidambaram, A.; Khivantsev, K.; Walter, E. D.; Graham, T. R.; Reardon, P.; Szanyi, J.; Fast, D. B.; Miller, Q. R. S.; Park, A.-H. A.; Stylianou, K. C. CO_2 Capture from Wet Flue Gas Using a Water-stable and Cost-effective Metal-organic Framework. *Cell Rep. Phys. Sci.* **2023**, *4* (7), No. 101470.
(27) Britt, D.; Furukawa, H.; Wang, B.; Glover, T. G.; Yaghi, O. M. Highly efficient separation of carbon dioxide by a metal-organic framework replete with open metal sites. *Proc. Natl. Acad. Sci.* **2009**, *106* (49), 20637−20640.
(28) Bao, Z.; Yu, L.; Ren, Q.; Lu, X.; Deng, S. Adsorption of CO_2 and CH_4 on a Magnesium-Based Metal Organic Framework. *J. Colloid Interface Sci.* **2011**, *353* (2), 549−556.
(29) Liang, W.; Coghlan, C. J.; Ragon, F.; Rubio-Martinez, M.; D'Alessandro, D. M.; Babarao, R. Defect Engineering of UiO-66 for CO_2 and H_2O Uptake − A Combined Experimental and Simulation Study. *Dalton Trans.* **2016**, *45* (11), 4496−4500.
(30) Chowdhury, P.; Bikkina, C.; Meister, D.; Dreisbach, F.; Gumma, S. Comparison of Adsorption Isotherms on Cu-BTC Metal Organic Frameworks Synthesized from Different Routes. *Microporous Mesoporous Mater.* **2009**, *117* (1), 406−413.
(31) Justin, A.; Espin, J.; Kochetygov, I.; Asgari, M.; Trukhina, O.; Queen, W. L. A Two Step Postsynthetic Modification Strategy: Appending Short Chain Polyamines to Zn-NH(2)-BDC MOF for Enhanced $CO_{(2)}$ Adsorption. *Inorg. Chem.* **2021**, *60* (16), 11720−11729.
(32) Torrisi, A.; Bell, R. G.; Mellot-Draznieks, C. Functionalized MOFs for Enhanced CO_2 Capture. *Cryst. Growth Des.* **2010**, *10* (7), 2839−2841.
(33) Jeoung, S.; Kim, S.; Kim, M.; Moon, H. R. Pore Engineering of Metal-organic Frameworks with Coordinating Functionalities. *Coord. Chem. Rev.* **2020**, *420*, No. 213377.
(34) Anderson, R.; Rodgers, J.; Argueta, E.; Biong, A.; Gómez-Gualdrón, D. A. Role of Pore Chemistry and Topology in the CO2 Capture Capabilities of MOFs: From Molecular Simulation to Machine Learning. *Chem. Mater.* **2018**, *30* (18), 6325−6337.
(35) Kalaj, M.; Cohen, S. M. Postsynthetic Modification: An Enabling Technology for the Advancement of Metal−organic Frameworks. *ACS Cent. Sci.* **2020**, *6* (7), 1046−1057.
(36) Wang, X.; Alzayer, M.; Shih, A. J.; Bose, S.; Xie, H.; Vornholt, S. M.; Malliakas, C. D.; Alhashem, H.; Joodaki, F.; Marzouk, S.; Xiong, G.; Del Campo, M.; Le Magueres, P.; Formalik, F.; Sengupta, D.; Idrees, K. B.; Ma, K.; Chen, Y.; Kirlikovali, K. O.; Islamoglu, T.; Chapman, K. W.; Snurr, R. Q.; Farha, O. K. Tailoring Hydrophobicity and Pore Environment in Physisorbents for Improved Carbon Dioxide Capture under High Humidity. *J. Am. Chem. Soc.* **2024**, *146* (6), 3943−3954.
(37) Ji, Z.; Wang, H.; Canossa, S.; Wuttke, S.; Yaghi, O. M. Pore Chemistry of Metal−organic Frameworks. *Adv. Funct. Mater.* **2020**, *30* (41), No. 2000238.
(38) Stein, A.; Wang, Z.; Fierke, M. A. Functionalization of Porous Carbon Materials with Designed Pore Architecture. *Adv. Mater.* **2009**, *21* (3), 265−293.
(39) Bose, S.; Sengupta, D.; Malliakas, C. D.; Idrees, K. B.; Xie, H.; Wang, X.; Barsoum, M. L.; Barker, N. M.; Dravid, V. P.; Islamoglu, T.; Farha, O. K. Suitability of a diamine functionalized metal−organic framework for direct air capture. *Chemical Science* **2023**, *14* (35), 9380−9388.
(40) Arstad, B.; Fjellvåg, H.; Kongshaug, K. O.; Swang, O.; Blom, R. Amine functionalised metal organic frameworks (MOFs) as adsorbents for carbon dioxide. *Adsorption* **2008**, *14* (6), 755−762.
(41) Si, X.; Jiao, C.; Li, F.; Zhang, J.; Wang, S.; Liu, S.; Li, Z.; Sun, L.; Xu, F.; Gabelica, Z.; Schick, C. High and Selective CO_2 Uptake, H2 Storage and Methanol Sensing on the Amine-Decorated 12-Connected MOF CAU-1. *Energy Environ. Sci.* **2011**, *4* (11), 4522−4527.
(42) An, J.; Geib, S. J.; Rosi, N. L. High and Selective CO_2 Uptake in a Cobalt Adeninate Metal−organic Framework Exhibiting Pyrimidine- and Amino-decorated Pores. *J. Am. Chem. Soc.* **2010**, *132* (1), 38−39.
(43) Stavitski, E.; Pidko, E. A.; Couck, S.; Remy, T.; Hensen, E. J. M.; Weckhuysen, B. M.; Denayer, J.; Gascon, J.; Kapteijn, F. Complexity behind CO_2 Capture on NH_2-MIL-53(Al). *Langmuir* **2011**, *27* (7), 3970−3976.
(44) Oliveira, A. S.; Rivero-Buceta, E. M.; Vidaurre-Agut, C.; Misturini, A.; Moreno, V.; Jorda, J. L.; Sastre, G.; Pergher, S. B. C.; Botella, P. Sequential pore wall functionalization in covalent organic frameworks and application to stable camptothecin delivery systems. *Mater. Sci. Eng. C Mater. Biol. Appl.* **2020**, *117*, No. 111263.
(45) Darunte, L. A.; Oetomo, A. D.; Walton, K. S.; Sholl, D. S.; Jones, C. W. Direct Air Capture of CO_2 Using Amine Functionalized MIL-101(Cr). *ACS Sustainable Chem. Eng.* **2016**, *4* (10), 5761−5768.
(46) Lyu, H.; Chen, O. I.-F.; Hanikel, N.; Hossain, M. I.; Flaig, R. W.; Pei, X.; Amin, A.; Doherty, M. D.; Impastato, R. K.; Glover, T. G.;

https://doi.org/10.1021/jacsau.4c00808
JACS Au 2024, 4, 4833−4843

Moore, D. R.; Yaghi, O. M. Carbon Dioxide Capture Chemistry of Amino Acid Functionalized Metal−Organic Frameworks in Humid Flue Gas. *J. Am. Chem. Soc.* **2022**, *144* (5), 2387−2396.
(47) Martell, J. D.; Zasada, L. B.; Forse, A. C.; Siegelman, R. L.; Gonzalez, M. I.; Oktawiec, J.; Runčevski, T.; Xu, J.; Srebro-Hooper, M.; Milner, P. J.; Colwell, K. A.; Autschbach, J.; Reimer, J. A.; Long, J. R. Enantioselective Recognition of Ammonium Carbamates in a Chiral Metal−organic Framework. *J. Am. Chem. Soc.* **2017**, *139* (44), 16000−16012.
(48) Mao, V. Y.; Milner, P. J.; Lee, J.-H.; Forse, A. C.; Kim, E. J.; Siegelman, R. L.; McGuirk, C. M.; Zasada, L. B.; Neaton, J. B.; Reimer, J. A.; Long, J. R. Cooperative Carbon Dioxide Adsorption in Alcoholamine- and Alkoxyalkylamine-functionalized Metal−organic Frameworks. *Angew. Chem., Int. Ed.* **2020**, *59* (44), 19468−19477.
(49) Forse, A. C.; Milner, P. J.; Lee, J.-H.; Redfearn, H. N.; Oktawiec, J.; Siegelman, R. L.; Martell, J. D.; Dinakar, B.; Zasada, L. B.; Gonzalez, M. I.; Neaton, J. B.; Long, J. R.; Reimer, J. A. Elucidating CO_2 Chemisorption in Diamine-appended Metal−organic Frameworks. *J. Am. Chem. Soc.* **2018**, *140* (51), 18016−18031.
(50) Gan, L.; Chidambaram, A.; Fonquernie, P. G.; Light, M. E.; Choquesillo-Lazarte, D.; Huang, H.; Solano, E.; Fraile, J.; Vinas, C.; Teixidor, F.; Navarro, J. A. R.; Stylianou, K. C.; Planas, J. G. A Highly Water-stable meta-Carborane-based Copper Metal-organic Framework for Efficient High-Temperature Butanol Separation. *J. Am. Chem. Soc.* **2020**, *142* (18), 8299−8311.
(51) Gan, L.; Andres-Garcia, E.; Mínguez Espallargas, G.; Planas, J. G. Adsorptive Separation of CO_2 by a Hydrophobic Carborane-Based Metal−Organic Framework under Humid Conditions. *ACS Appl. Mater. Interfaces* **2023**, *15* (4), 5309−5316.
(52) Dolomanov, O. V.; Bourhis, L. J.; Gildea, R. J.; Howard, J. A. K.; Puschmann, H. OLEX2: a complete structure solution, refinement and analysis program. *J. Appl. Crystallogr.* **2009**, *42* (2), 339−341.
(53) Kim, H. K.; Yun, W. S.; Kim, M.-B.; Kim, J. Y.; Bae, Y.-S.; Lee, J.; Jeong, N. C. A Chemical Route to Activation of Open Metal Sites in the Copper-Based Metal−Organic Framework Materials HKUST-1 and Cu-MOF-2. *J. Am. Chem. Soc.* **2015**, *137* (31), 10009−10015.
(54) Chen, Y.; Mu, X.; Lester, E.; Wu, T. High Efficiency Synthesis of HKUST-1 Under Mild Conditions with High BET Surface Area and CO_2 Uptake Capacity. *Prog. Nat. Sci. Mater. Int.* **2018**, *28* (5), 584−589.
(55) Al-Janabi, N.; Hill, P.; Torrente-Murciano, L.; Garforth, A.; Gorgojo, P.; Siperstein, F.; Fan, X. Mapping the Cu-BTC Metal−organic Framework (HKUST-1) Stability Envelope in the Presence of Water Vapour for CO2 Adsorption from Flue Gases. *Chem. Eng. J.* **2015**, *281*, 669−677.
(56) Gładysiak, A.; Nguyen, T. N.; Navarro, J. A. R.; Rosseinsky, M. J.; Stylianou, K. C. A Recyclable Metal−organic Framework as a Dual Detector and Adsorbent for Ammonia. *Chem.—Eur. J.* **2017**, *23* (55), 13602−13606.
(57) Soubeyrand-Lenoir, E.; Vagner, C.; Yoon, J. W.; Bazin, P.; Ragon, F.; Hwang, Y. K.; Serre, C.; Chang, J.-S.; Llewellyn, P. L. How Water Fosters a Remarkable 5-Fold Increase in Low-pressure CO_2 Uptake within Mesoporous MIL-100(Fe). *J. Am. Chem. Soc.* **2012**, *134* (24), 10174−10181.
(58) Rieth, A. J.; Dincă, M. Controlled Gas Uptake in Metal−organic Frameworks with Record Ammonia Sorption. *J. Am. Chem. Soc.* **2018**, *140* (9), 3461−3466.
(59) Moribe, S.; Chen, Z.; Alayoglu, S.; Syed, Z. H.; Islamoglu, T.; Farha, O. K. Ammonia Capture within Isoreticular Metal−organic Frameworks with Rod Secondary Building Units. *ACS mater. lett.* **2019**, *1* (4), 476−480.
(60) Zhang, D.; Shen, Y.; Ding, J.; Zhou, H.; Zhang, Y.; Feng, Q.; Zhang, X.; Chen, K.; Wang, J.; Chen, Q.; Zhang, Y.; Li, C. Tunable Ammonia Adsorption within Metal−Organic Frameworks with Different Unsaturated Metal Sites. *Molecules* **2022**, *27* (22), 7847.
(61) Lyu, P.; Wright, A. M.; López-Olvera, A.; Mileo, P. G. M.; Zárate, J. A.; Martínez-Ahumada, E.; Martis, V.; Williams, D. R.; Dincă, M.; Ibarra, I. A.; Maurin, G. Ammonia Capture via an Unconventional Reversible Guest-induced Metal-linker Bond Dynamics in a Highly Stable Metal−organic Framework. *Chem. Mater.* **2021**, *33* (15), 6186−6192.
(62) Zhu, Z.; Wang, H.; Wu, X.-Y.; Luo, K.; Fan, J. Computational Screening of Metal−Organic Frameworks for Ammonia Capture from H2/N2/NH3Mixtures. *ACS Omega* **2022**, *7* (42), 37640−37653.
(63) Guo, L.; Hurd, J.; He, M.; Lu, W.; Li, J.; Crawshaw, D.; Fan, M.; Sapchenko, S.; Chen, Y.; Zeng, X.; Kippax-Jones, M.; Huang, W.; Zhu, Z.; Manuel, P.; Frogley, M. D.; Lee, D.; Schröder, M.; Yang, S. Efficient Capture and Storage of Ammonia in Robust Aluminium-based Metal-organic Frameworks. *Commun. Chem.* **2023**, *6* (1), 55.
(64) Carné-Sánchez, A.; Martínez-Esaín, J.; Rookard, T.; Flood, C. J.; Faraudo, J.; Stylianou, K. C.; Maspoch, D. Ammonia Capture in Rhodium(II)-Based Metal−Organic Polyhedra via Synergistic Coordinative and H-Bonding Interactions. *ACS Appl. Mater. Interfaces* **2023**, *15* (5), 6747−6754.
(65) Britt, D.; Tranchemontagne, D.; Yaghi, O. M. Metal-organic frameworks with high capacity and selectivity for harmful gases. *Proc. Natl. Acad. Sci.* **2008**, *105* (33), 11623−11627.
(66) Rieth, A. J.; Tulchinsky, Y.; Dinca, M. High and Reversible Ammonia Uptake in Mesoporous Azolate Metal-Organic Frameworks with Open Mn, Co, and Ni Sites. *J. Am. Chem. Soc.* **2016**, *138* (30), 9401−4.
(67) Han, X.; Lu, W.; Chen, Y.; da Silva, I.; Li, J.; Lin, L.; Li, W.; Sheveleva, A. M.; Godfrey, H. G. W.; Lu, Z.; Tuna, F.; McInnes, E. J. L.; Cheng, Y.; Daemen, L. L.; McPherson, L. J. M.; Teat, S. J.; Frogley, M. D.; Rudić, S.; Manuel, P.; Ramirez-Cuesta, A. J.; Yang, S.; Schröder, M. High Ammonia Adsorption in MFM-300 Materials: Dynamics and Charge Transfer in Host-guest Binding. *J. Am. Chem. Soc.* **2021**, *143* (8), 3153−3161.
(68) Ma, X.; Li, L.; Wang, S.; Lu, M.; Li, H.; Ma, W.; Keener, T. C. Ammonia-treated Porous Carbon Derived from ZIF-8 for Enhanced CO_2 Adsorption. *Appl. Surf. Sci.* **2016**, *369*, 390−397.
(69) Kim, E. J.; Siegelman, R. L.; Jiang, H. Z. H.; Forse, A. C.; Lee, J.-H.; Martell, J. D.; Milner, P. J.; Falkowski, J. M.; Neaton, J. B.; Reimer, J. A.; Weston, S. C.; Long, J. R. Cooperative carbon capture and steam regeneration with tetraamine-appended metal−organic frameworks. *Science* **2020**, *369* (6502), 392−396.
(70) Suffren, Y.; Rollet, F.-G.; Reber, C. Raman Spectroscopy of Transition Metal Complexes: Molecular Vibrational Frequencies, Phase Transitions, Isomers, and Electronic Structure. *Comments on Inorg. Chem.* **2011**, *32* (5−6), 246−276.
(71) Hamed, F. A. E.; Yasin, S. I.; Ali, M. S. The Removal of Some Metals by Natural and Modified Zeolite from Produced Water. *J. Basic Appl. Chem.* **2015**, *5*, 16−22.
(72) Haque, N.; Biswas, S.; Basu, P.; Haque Biswas, I.; Khatun, R.; Khan, A.; Islam, S. M. Triazinetriamine-derived Porous Organic Polymer-supported Copper Nanoparticles (Cu-NPs@TzTa-POP): An Efficient Catalyst for the Synthesis of N-methylated Products via CO_2 Fixation and Primary Carbamates from Alcohols and Urea. *New J. Chem.* **2020**, *44* (36), 15446−15458.
(73) Bacsik, Z.; Zhang, P.; Hedin, N. Ammonium-Carbamate-Rich Organogels for the Preparation of Amorphous Calcium Carbonates. *Minerals* **2017**, *7* (7), 110.
(74) Stylianou, K. C.; Heck, R.; Chong, S. Y.; Bacsa, J.; Jones, J. T. A.; Khimyak, Y. Z.; Bradshaw, D.; Rosseinsky, M. J. A Guest-Responsive Fluorescent 3D Microporous Metal−organic Framework Derived from a Long-lifetime Pyrene Core. *J. Am. Chem. Soc.* **2010**, *132* (12), 4119−4130.
(75) Stylianou, K. C.; Rabone, J.; Chong, S. Y.; Heck, R.; Armstrong, J.; Wiper, P. V.; Jelfs, K. E.; Zlatogorsky, S.; Bacsa, J.; McLennan, A. G.; Ireland, C. P.; Khimyak, Y. Z.; Thomas, K. M.; Bradshaw, D.; Rosseinsky, M. J. Dimensionality Transformation through Paddle-wheel Reconfiguration in a Flexible and Porous Zn-based Metal−organic Framework. *J. Am. Chem. Soc.* **2012**, *134* (50), 20466−20478.
(76) Lee, E. Y.; Jang, S. Y.; Suh, M. P. Multifunctionality and Crystal Dynamics of a Highly Stable, Porous Metal−organic Framework $[Zn_4O(NTB)_2]$. *J. Am. Chem. Soc.* **2005**, *127* (17), 6374−6381.
(77) Mao, H.; Tang, J.; Day, G. S.; Peng, Y.; Wang, H.; Xiao, X.; Yang, Y.; Jiang, Y.; Chen, S.; Halat, D. M.; Lund, A.; Lv, X.; Zhang,

https://doi.org/10.1021/jacsau.4c00808
JACS Au 2024, 4, 4833−4843

W.; Yang, C.; Lin, Z.; Zhou, H.-C.; Pines, A.; Cui, Y.; Reimer, J. A. A Scalable Solid-state Nanoporous Network with Atomic-level Interaction Design for Carbon Dioxide Capture. *Sci. Adv.* **2022**, *8* (31), No. eabo6849.

(78) Alkhabbaz, M. A.; Bollini, P.; Foo, G. S.; Sievers, C.; Jones, C. W. Important Roles of Enthalpic and Entropic Contributions to CO_2 Capture from Simulated Flue Gas and Ambient Air Using Mesoporous Silica Grafted Amines. *J. Am. Chem. Soc.* **2014**, *136* (38), 13170−13173.

(79) McDonald, T. M.; Mason, J. A.; Kong, X.; Bloch, E. D.; Gygi, D.; Dani, A.; Crocellà, V.; Giordanino, F.; Odoh, S. O.; Drisdell, W. S.; Vlaisavljevich, B.; Dzubak, A. L.; Poloni, R.; Schnell, S. K.; Planas, N.; Lee, K.; Pascal, T.; Wan, L. F.; Prendergast, D.; Neaton, J. B.; Smit, B.; Kortright, J. B.; Gagliardi, L.; Bordiga, S.; Reimer, J. A.; Long, J. R. Cooperative insertion of CO_2 in diamine-appended metal-organic frameworks. *Nature* **2015**, *519* (7543), 303−308.

(80) Siegelman, R. L.; McDonald, T. M.; Gonzalez, M. I.; Martell, J. D.; Milner, P. J.; Mason, J. A.; Berger, A. H.; Bhown, A. S.; Long, J. R. Controlling Cooperative CO_2 Adsorption in Diamine-appended Mg_2(dobpdc) Metal−organic Frameworks. *J. Am. Chem. Soc.* **2017**, *139* (30), 10526−10538.

(81) Flaig, R. W.; Osborn Popp, T. M.; Fracaroli, A. M.; Kapustin, E. A.; Kalmutzki, M. J.; Altamimi, R. M.; Fathieh, F.; Reimer, J. A.; Yaghi, O. M. The Chemistry of CO_2 Capture in an Amine-Functionalized Metal−organic Framework under Dry and Humid Conditions. *J. Am. Chem. Soc.* **2017**, *139* (35), 12125−12128.

(82) Vitillo, J. G.; Ricchiardi, G. Effect of Pore Size, Solvation, and Defectivity on the Perturbation of Adsorbates in MOFs: The Paradigmatic Mg_2(dobpdc) Case Study. *J. Phys. Chem. C* **2017**, *121* (41), 22762−22772.

(83) Yadav, A. K.; Gladysiak, A.; Song, A.; Gan, L.; Simons, C. R.; Alghoraibi, N. M.; Alahmed, A. H.; Mourad, Y.; Reimer, J. A.; Huang, H.; Planas, J. G.; Stylianou, K. C.Solid-state NMR data from: Sequential Pore Functionalization in MOFs for Enhanced Carbon Dioxide Capture [Dataset]. *Dryad*. https://doi.org/10.5061/dryad.v15dv426b.

https://doi.org/10.1021/jacsau.4c00808
JACS Au 2024, 4, 4833−4843